Final Response

Dear Editor,

Firstly, we wish to thank you and the reviewers for your continued patience throughout this review process and for agreeing to extend the deadline for such a long period of time. This request was due to myself taking an extended and unexpectedly early maternity leave and as a co-author team we decided it would be better to wait until my return to work to respond to the reviews.

We are grateful to both reviewers for their constructive comments on our manuscript. Please find in this final response a point-by-point reply to all reviewer comments (red text), including the changes we have made to the manuscript (marked in italics). The revised manuscript is attached below the response to the reviewers.

Kind Regards

Grace Nield

Response to Reviewer 1

The authors used ABAQUS —a commercial finite-element software package— to simulate postseismic deformation on the self-gravitating earth model. They have benchmarked their results for both coseismic and postseismic deformations with semianalytical solutions.

The article's subject matter is interesting and relevant to the journal of Geoscientific Model Development (GMD). The results for the given examples look excellent. I have the impression that the overall content of the article could be improved. I have a few concerns.

We thank the reviewer for these helpful comments and have responded in line below.

- The authors used the finite-element method, which is also clearly implied from the title. However, I do not see any related finite element formulations. I expect at least the strong and weak forms of the governing equations with necessary boundary conditions so that the work is entirely reproducible. For example, implementing full gravity and solid-fluid coupling is known to be challenging for global problems. I am curious about how those aspects are implemented. In my view, a proper section for appropriate formulations would make this article complete.

We have not included the governing equations for the finite element formulation as this part of the study is not new work. The model is based on the finite element formulation of Wu (2004) and equations therein, as referenced on line 84. Instead, we focus the paper on describing the new aspects of this model – incorporating a fault plane and prescribing slip. To make the work more reproducible we have added further references to Wu (2004) through Section 2.3 as follows:

*We follow the approach described in Section 4.1 of Wu (2004) and apply elastic foundations (ABAQUS keyword *Foundation) to each layer boundary with a material density contrast occurring across it (including the surface and core-mantle-boundary). This means that advection of pre-stress is included and takes care of the restoring forces of buoyancy neglected in a conventional finite-element model (Wu, 2004, equation 3). The elastic foundations have a stiffness equal to the difference in density multiplied by gravitational acceleration (see Wu (2004) equations 12a,b,c).*

- The most basic and widely used Earth model is the Preliminary reference Earth model (PREM, Dziewonski, A. M. & Anderson, D. L., 1981). I wonder why authors chose to use a simple three-layered model instead of the PREM. Furthermore, they mention in the abstract "the model can be easily adapted to include different rheological models and lateral variations". In this context, at least one example with the lateral variation of viscosity (e.g., Latychev et al., 2005) would be interesting.

We chose the same simple three-layer structure for this benchmarking exercise as that used by Pollitz (1997) (line 186). Since we were undertaking some benchmarking tests with the same fault geometry as those in Pollitz (1997) it was essential to keep the Earth model consistent with that study. Using the Preliminary Reference Earth Model (PREM) instead would not add anything to the results in our opinion, and only complicate reproducibility of the results for others.

We have added a sentence to new line 210 to explain:

We use a simple Earth structure rather than the Preliminary Reference Earth Structure (PREM, Dziewonski & Anderson, 1981) to ensure our results are consistent with Pollitz (1997).

Our study does not include lateral variations in viscosity as the primary aim was to benchmark the model against other existing models and there is no open-source spherical model that we are aware of with which to benchmark these results. Using the model for case studies that require lateral variations in viscosity will be the subject of future work.

- Although not explained in the article, it seems that the mesh contains the nonconforming elements when transitioning from course to fine elements as shown in Figure 1. But then in Section "2.1 Model Geometry and Mesh" the authors mention, "The element type used is an 8-node linear brick element"! How is it possible to use an 8- node brick element for nonconforming elements? Do you use a discontinuous Galerkin method? Please clarify.

We thank the reviewer for bringing to our attention this lack of detail. ABAQUS provides a useful way to join together meshes of different resolutions to aid mesh refinement problems. The two separate meshes are joined together by a "tie constraint" on a surface where they have non-conforming elements relative to each other. Using a tie constraint ensures there is no relative movement between the surfaces and that displacement and stress are continuous through the boundaries. Nodes on one mesh are tied to nodes on the other mesh. Tie coefficients are generated and used to interpolate quantities from nodes on one side of the mesh to nodes on the other side of the mesh. We have expanded the text in Section 2.1 to include further description of this method as below:

*The two parts are then tied together (ABAQUS keyword *Tie) using surface-to-surface tie constraints. This means that although the two separate meshes have non-conforming elements relative to each other, the tie constraints ensure there is no relative movement between the surfaces and that displacement and stress are continuous through the boundaries. Tie coefficients are generated and used to interpolate quantities from nodes on one side of the mesh to nodes on the other side of the mesh.*

- Authors have frequently used the term "flat earth." I think "homogeneous halfspace" or "layered halfspace" is probably a more appropriate term.

We will change this term to "layered halfspace" but will also note on first use that it is also referred to as "flat-Earth" in other literature (e.g. Wu, 2004) so as not to cause confusion to the reader.

Given the above comments, I would recommend this article for a moderate to major revision. Minor comments follow. In the comments below, P refers to the page number, and L refers to the line number.

P4L29: "..on the likely Earth structure..." What do you mean by "likely Earth structure"?

We mean Earth structure inferred by the model. We will change this to "inferred Earth structure".

P2L34: "flat-Earth." "Homogeneous halfspace" or "layered halfspace"?

We will change this term to "layered halfspace".

P3L92: "a fault plane within the mesh." Given that you use the brick elements, accommodating the realistic and complex faults may be very difficult with this approach. Alternatively, one can use the so-called moment-density tensor approach.

We acknowledge that a limitation of the model is that it is currently restricted to a single fault plane, due to the difficulties in constructing a mesh around a complex fault structure, as discussed on line 246. The moment-density tensor approach suggested by the reviewer is an alternative method of representing a fault within a spectral-element mesh (e.g. Gharti et al. 2019) whereby the mesh geometry is not required to conform to the geometry of the fault plane. However, our current knowledge is that this method cannot be implemented in a finite-element mesh in ABAQUS due to the restrictions of defining loads and forces on elements or surfaces within the mesh. The focus of our study is far-field deformation which is not sensitive to the details of the fault plane and slip distribution (Khazaradze et al., 2002, Tregoning et al., 2013, Zhou et al. 2012), rather it is the overall moment magnitude that is important, which can be represented on a single plane. We have included additional text in the discussion as follows:

In the case of a fault inversion that suggests multiple fault segments (e.g. Ye et al., 2014), an approximation of all the fault planes into a single geometry could still provide a realistic far-field estimate of postseismic deformation (e.g. Takeuchi and Fialko, 2013), particularly if the fault geometry and slip are adjusted so that model output matches observations of coseismic displacement (e.g. Sun et al., 2018). Far-field postseismic deformation is less sensitive to simplifications made to the fault geometry and slip

distribution than near-field deformation (Khazaradze et al., 2002, Tregoning et al., 2013, Zhou et al. 2012).

P3L96: "...using surface-to-surface tie constraints. . ." Please write appropriate equations for these constraints.

The equations used by ABAQUS to define the tie constraints are integrated into the software so it would not be appropriate to reproduce them in this paper. The information we have included with regards to ABAQUS key words and input files is sufficient to allow other to use these methods.

P4 Section 2.3: These boundary conditions are best to be represented by appropriate equations!

We will include a more specific reference to the Wu (2004) study that this model is based on so that the reader can refer to the original source for the equations. Please also refer back to our response to the earlier comment.

P6L165: "...as the fault is not allowed to open." Realistic faults may have some opening as well. How do you accommodate that kind of scenario?

At present we do not accommodate opening faults although we appreciate this is a realistic fault scenario. We recognise that this is a limitation of our model and have included a further comment in the discussion section (new line 279) to acknowledge this.

At present the fault is not permitted to open, and whilst this is a realistic scenario for a fault, it would have negligible impact on the far-field postseismic deformation.

P6L181: "500 km." Given that the total depth of the model is 670 km, how does this large element behave?

The total depth of the model is 2891 km – from the surface down to the lower mantle-core boundary. The elements of 500 km size are present only within the lower mantle layer and the global mesh that surrounds the region of refined mesh where the fault lies. We ensure that the majority of coseismic and postseismic displacement occurs in the inner part of the model where elements are much smaller, so that the large elements should be deforming by only a negligible amount.

P7L185: "... simple Earth structure". Why not use a more common Earth model PREM?

Please see response to earlier comment about the use of PREM.

P7 Section 4.2 Coseismic Results Can you show the snapshots of the surface displacement?

We have added 3 new figures to Appendix B showing coseismic surface displacement and postseismic surface displacement at the 3 times shown in profiles on figures 3-5. The 3 new figures correspond to the fault geometries tested.

P7 Section 4.3 Postseismic Results Can you show the snapshots of the surface displacement at selected time steps?

Please see response to previous comment.

P7L214: "...less coseimic dispalcemetn from the ABAQUS. . ." What is the reason for less coseismic displacement for ABAQUS?

We attribute this to mesh issues, as detailed on line 205 (new line 227). We have now included more details on mesh resolution tests as suggested by reviewer 2, which provides further justification. The text in Section 4.3 has been amended as follows:

> *The mismatch in the coseismic displacement due to limitations in mesh resolution is the cause of mismatch for the postseismic displacement, i.e., less coseismic displacement from the ABAQUS model would result in less stress and therefore less relaxation. Slight improvements in the near-field displacement could be made by increasing the mesh resolution in the vicinity of the fault but would come at a computational cost (see Appendix A).*

P9L251: "...an approximation of all the fault planes into a single geometry would be required.." I don't think this is a reliable way. A better alternative is to use the moment density tensor approach.

Please refer to our earlier comment and manuscript edits regarding the moment-density tensor approach. We agree that in the near-field results would not be as reliable as fully representing the structure, however, representing complex fault geometry with a single plane geometry can provide a useful way of modelling far-field postseismic deformation. This method has been used by Takeuchi and Fialko (2013), and we will include a reference to this study on line 251 (new line 277).

Figure 1: This figure may be sharper and better in black and white.

When outputting graphics from ABAQUS in black and white the quality is worse. We will keep the colour but output at higher resolution.

Figures 3-5: Showing the depth only to 100 km is confusing. Either show the full depth or explain it in the captions.

We show the upper 100km as these material properties are those that primarily govern the Earth's response, but we agree this could be confusing. We have changed the caption to include the following sentence:

> *Top panels of a) and b) show the fault dimensions and material properties of the upper 100 km of the model. Layers and material properties below 100 km depth are given in Table 2.*

Figures 3-7: Figures look low in quality. It may be better to save those figures in vector graphics, if possible.

Figures 3-7 will be submitted as vector graphics with the final manuscript.

Finally, the following references are worth citing. References: Al-Attar, D. & Tromp, J., 2014: Sensitivity kernels for viscoelastic loading based on adjoint methods Geophysical Journal International, Oxford University Press, 196, 34-77

Dziewonski, A. M. & Anderson, D. L., 1981: Preliminary reference Earth model Physics of the Earth and Planetary Interiors, 25, 297-356

Latychev, K.; Mitrovica, J. X.; Tromp, J.; Tamisiea, M. E.; Komatitsch, D. & Christara, C. C., 2005: Glacial isostatic adjustment on 3-D Earth models: a finite-volume formulation Geophysical Journal International, Blackwell Science Ltd, 161, 421-444

Zhong, S.; Paulson, A. & Wahr, J., 2003: Three-dimensional finite-element modelling of Earth's viscoelastic deformation: effects of lateral variations in lithospheric thickness Geophysical Journal International, 155, 679-695

We thank the reviewer for suggesting further references and will include them as appropriate in the text.

Additional References:

Gharti, H. N., Langer, L., and Tromp, J., 2019. Spectral-infinite-element simulations of earthquake-induced gravity perturbations, Geophysical Journal International, 217, 451-468. DOI:10.1093/gji/ggz028.

Khazaradze, G., Wang, K., Klotz, J., Hu, Y., and He, J., Prolonged post-seismic deformation of the 1960 great Chile earthquake and implications for mantle rheology, Geophys. Res. Lett., 29(22), 2050, doi:10.1029/2002GL015986, 2002.

Tregoning, P., Burgette, R., McClusky, S. C., Lejeune, S., Watson, C. S., and McQueen, H. (2013), A decade of horizontal deformation from great earthquakes, J. Geophys. Res. Solid Earth, 118, 2371– 2381, doi:10.1002/jgrb.50154.

Zhou, X., Sun, W., Zhao, B., Fu, G., Dong, J., and Nie, Z. (2012), Geodetic observations detecting coseismic displacements and gravity changes caused by the Mw = 9.0 Tohoku-Oki earthquake, J. Geophys. Res., 117, B05408, doi:10.1029/2011JB008849.

Response to Reviewer 2

Review of "A global, spherical, finite-element model for postseismic deformation using ABAQUS" by Nield and co-authors.

We thank the reviewer for these suggestions and have responded to the detailed comments in line below.

The manuscript represents an implementation of postseismic viscoelastic relaxation problems in a widely used finite-element commercial package. The study addresses common problems associated with meshing the domain, which is difficult around faults, and benchmarks the results against semi-analytic solutions attained with another widely used, but open-source, package. The study is accompanied with supplementary material that allows the community to reproduce and expand on these results quickly.

The study makes a number of simplifying assumptions about the rheology of the Earth that permits direct comparison with the semi-analytic code visco1d. However, once the code is benchmarked, these assumptions should be relaxed and more realistic constitutive laws that include a power-law stress/strain-rate relationship at steady state and a similar power-law constitutive behavior for transient creep - all compatible with laboratory observation of olivine creep - should be implemented and described. More realistic distributions of physical properties associated with thermal activation of viscoelastic flow in a realistic thermal field should follow.

Power-law and transient power-law rheology have not been included in this study as the primary aim is to benchmark coseismic and postseismic displacement results against those produced by existing models with linear rheology. The implementation in ABAQUS of the rheologies mentioned by the reviewer is straight forward and has been done in other studies as mentioned on line 108. We have added more detail and references such as those suggested by the reviewer in their later comment to section 2.2 to expand on this (see extract below). However, using our model with more complex rheology will be the subject of future work and we feel that this is outside of the scope of our benchmarking study.

> *In this study we limit our benchmarking examples to a 1D linear viscoelastic rheology with one (Maxwell) or two (Burgers) relaxation times, however ABAQUS has the capability of implementing a variety of rheological models, including user-specified constitutive equations. For example, Freed et al. (2012) combined power-law rheology with a transient phase to model postseismic deformation following the 1999 magnitude 7.1 Hector Mine earthquake, and van der Wal et al. (2010) used a composite rheology based on laboratory-derived flow laws for diffusion and dislocation creep (Hirth and Kohlstedt, 2003; Karato and Wu, 1993) to model global glacial isostatic adjustment. Furthermore, variations of our model could be constructed using a 3D Earth structure (e.g. van der Wal et al., 2015).*

A remaining issue is the meshing around more complex fault assembly that include multiple surfaces is not included in the model. As many earthquakes are now imaged to such a level of accuracy that these details are often well constrained, including complex fault geometry would be a relevant addition.

We agree this remains a limitation of the model due to the difficulties in constructing a mesh around a complex fault structure with brick elements. However, we are focusing on the far-field postseismic displacement which is

less sensitive to simplifications made to the fault geometry than near-field displacement (Khazaradze et al., 2002, Tregoning et al., 2013, Zhou et al. 2012). Representing complex fault geometry with a single plane geometry can provide a useful way of modelling far-field postseismic deformation. This method has been used by Takeuchi and Fialko (2013), and we will include a reference to this study on line 251 (new line 277). When applied to case studies, fault and slip properties in the model can be adjusted so that model output matches observations of coseismic displacements which provides further confidence in modelled far-field deformations (e.g. Sun et al., 2018). We have amended the text in the discussion section to reflect these points:

> *In the case of a fault inversion that suggests multiple fault segments (e.g. Ye et al., 2014), an approximation of all the fault planes into a single geometry could still provide a realistic far-field estimate of postseismic deformation (e.g. Takeuchi and Fialko, 2013), particularly if the fault geometry and slip are adjusted so that model output matches observations of coseismic displacement (e.g. Sun et al., 2018). Far-field postseismic deformation is less sensitive to simplifications made to the fault geometry and slip distribution than near-field deformation (Khazaradze et al., 2002, Tregoning et al., 2013, Zhou et al. 2012).*

Finally, the iterative procedure to include self-gravity should be replaced by directly solving the appropriate equations based on advection of pre-stress.

This approach is not possible for a spherical model in ABAQUS, please also see more detailed response to comment below.

I follow with a few detailed remarks.

55: An example of finite-element modeling of post-seismic relaxation with a spherical geometry is

Agata, R., Barbot, S.D., Fujita, K., Hyodo, M., Iinuma, T., Nakata, R., Ichimura, T. and Hori, T., 2019. Rapid mantle flow with power-law creep explains deformation after the 2011 Tohoku mega-quake.ÂaNature communications,Â ˇ a10(1), pp.1-11. ˇ

This additional reference will be included.

105: Since it seems so easy to add more realistic rheology with the method, it should actually be done in this study. More realistic rheology involves a power-law stress/strain-rate relationship, see

Hirth, G. and Kohlstedt, D.L., 2003. Rheology of the Upper Mantle and the Mantle Wedge: A View from the Experimentalists: Inside the Subduction Factory, v. 138.
Karato, S.I. and Wu, P., 1993. Rheology of the upper mantle: A synthesis. Science, C2 GMDD Interactive comment Printer-friendly version Discussion paper 260(5109), pp.771-778.
Recent development include the inclusion of transient creep compatible with nonlinear steady-state creep: Masuti, S., Barbot, S.D., Karato, S.I., Feng, L. and Banerjee, P., 2016. Upper-mantle water stratification inferred from observations of the 2012 Indian Ocean earthquake. Nature, 538(7625), pp.373-377.
Inclusion of realistic rheology seems more important and relevant than including selfgravitation.

We feel this is outside the scope of the benchmarking study, please also refer to our earlier comment.

130: It is unfortunate that Abaqus cannot simply solve the appropriate governing equations for self-gravitation and that these iterations are necessary. How can that be improved? Is there a way to solve a user-defined set of equations? Are the governing equations with self-gravitation not readily included in Abaqus? How is advection of pre-stress included?

The governing equations solved in ABAQUS cannot be changed. A gravity load can be included directly within ABAQUS as a uniform acceleration in one fixed direction, therefore it is not easily applied to a spherical model. We choose instead to use the iterative approach as this has been shown by others (Wu, 2004) to correctly represent self-gravitation for a spherical viscoelastic Earth.

Advection of pre-stress is included via the elastic foundations described in section 2.3. We have added additional text and references to Wu (2004) to this section to clarify.

> *This means that advection of pre-stress is included and takes care of the restoring forces of buoyancy neglected in a conventional finite-element model (Wu, 2004, equation 3). The elastic foundations have a stiffness equal to the difference in density multiplied by gravitational acceleration (see Wu (2004) equations 12a,b,c).*

180: The horizontal and vertical resolutions of the mesh seem inadequate to resolve the near field. The fault is 200x20 km and the mesh size around it is 10x5 km, representing just 20x4 mesh elements along the fault. It is actually surprising that the numerical result match the analytic solution so well with such a coarse mesh. This is perhaps an area of improvement.

We are focusing on the far-field postseismic deformation within a global setting, which requires a mesh with a very large number of elements. It is therefore computationally expensive to have a very high-resolution mesh in the near-field and we are forced to trade off the mesh resolution (and hence more accurate near-field results) against computation time. To provide further justification for our choice of mesh resolution we have performed extra sensitivity tests for one of the fault cases and included the results as Appendix A. We have summarised the results in the text in Section 4.1 as follows:

> *For the 30° dipping reverse fault we tested a coarser and a finer mesh and found that our chosen mesh resolution provided a satisfactory trade-off between computation time and accuracy, with the finer mesh giving only small differences in near-field displacement compared to our chosen mesh, for a 10-fold increase in computation time. The results of this sensitivity test are discussed in more detail in Appendix A.*

215: We need to see a convergence test in terms of mesh resolution for these cases. This may not necessitate more figures, but this needs to be discussed. I suspect that the resolution of the mesh in the near field can be improved, with valuable gains on the misfit. I suspect that the discrepancies that accumulate at long period during postseismic relaxation may be reduced with a more appropriate mesh in the near field.

As per our response to the previous comment, we have performed extra sensitivity tests for mesh resolution and summarised the results in the text. A more detailed description of the test and results has been included as a new Appendix (A).

250: If linear rheology models are assumed, several simulations can be run with separate parts of a complex fault geometry model - each fault at a time - and the results subsequently combined.

This is an approach that could work for modelling complex faults with linear rheology, we have included the following sentence in the discussion section to include this point.

> *Alternatively, each fault segment could be analysed in a separate model and resulting deformation be combined, providing a linear rheology is used.*

Additional References:

Khazaradze, G., Wang, K., Klotz, J., Hu, Y., and He, J., Prolonged post-seismic deformation of the 1960 great Chile earthquake and implications for mantle rheology, Geophys. Res. Lett., 29(22), 2050, doi:10.1029/2002GL015986, 2002.

Sun, T., Wang, K. & He, J., 2018. Crustal Deformation Following Great Subduction Earthquakes Controlled by Earthquake Size and Mantle Rheology, Journal of Geophysical Research: Solid Earth, 123, 5323-5345.

Tregoning, P., Burgette, R., McClusky, S. C., Lejeune, S., Watson, C. S., and McQueen, H. (2013), A decade of horizontal deformation from great earthquakes, J. Geophys. Res. Solid Earth, 118, 2371– 2381, doi:10.1002/jgrb.50154.

Zhou, X., Sun, W., Zhao, B., Fu, G., Dong, J., and Nie, Z. (2012), Geodetic observations detecting coseismic displacements and gravity changes caused by the Mw = 9.0 Tohoku-Oki earthquake, J. Geophys. Res., 117, B05408, doi:10.1029/2011JB008849.

A global, spherical, finite-element model for postseismic deformation using ABAQUS

Grace A. Nield[1,2], Matt A. King[1], Rebekka Steffen[3], Bas Blank[4]

[1]Surveying and Spatial Sciences, School of Technology, Environments and Design, University of Tasmania, Australia
[2]Department of Geography, Durham University, Durham, UK.
[3]Lantmäteriet, Gävle, Sweden
[4]Faculty of Aerospace Engineering, Delft University of Technology, Delft, NL

Correspondence to: Grace A. Nield (grace.a.nield@durham.ac.uk)

Abstract. We present a finite-element model of postseismic solid Earth deformation built in the software package ABAQUS (version 2018). The model is global and spherical, and includes self-gravitation and is built for the purpose of calculating postseismic deformation in the far-field (>~300km) of major earthquakes. An earthquake is simulated by prescribing slip on a fault plane in the mesh and the model relaxes under the resulting change in stress. Both linear Maxwell and biviscous (Burgers) rheological models have been implemented and the model can be easily adapted to include different rheological models and lateral variations in Earth structure, a particular advantage over existing models. We benchmark the model against an analytical coseismic solution and an existing open-source postseismic model, demonstrating good agreement for all fault geometries tested. Due to the inclusion of self-gravity the model has the potential for predicting deformation in response to multiple sources of stress change, for example, changing ice thickness in tectonically active regions.

1 Introduction

Earthquakes cause deformation at the Earth's surface from the immediate coseismic fault slip and, thereafter, from several processes. Afterslip on the fault on or near the rupture zone (e.g. Huang et al., 2014) and poroelastic relaxation due to changes in fluid pressure (e.g. Masterlark and Wang, 2002) result in deformation of near-field locations (typically <300km from the fault). As the Earth responds to stress changes associated with the earthquake, the lower crust and upper mantle undergo prolonged postseismic viscoelastic deformation. This is the dominant mode of displacement in the far-field and, for very large earthquakes (> magnitude 9), this can be observed geodetically over 1000 km from the earthquake source (Shao et al., 2016) and be sustained over decades. For example, deformation from the 1960 magnitude 9.5 Chile earthquake was still being observed ~40 years after the event (Khazaradze and Klotz, 2003). Postseismic deformation can be observed by increasingly dense networks of geodetic measurements such as GPS (e.g. Freed et al., 2012) and InSAR (e.g. Wang and Fialko, 2018) motivating the development of models to help interpret geodetically-observed deformation. The study of postseismic deformation can provide useful information about the Earth and can be used to place constraints on the ~~likely~~ inferred Earth structure (Pollitz, 2005) or rheology (Freed et al., 2012). It is important to be able to accurately quantify postseismic

deformation in regions where deformation occurs as a result of multiple sources, for example in Alaska where the Earth is also deforming in response to a changing ice load (Suito and Freymueller, 2009).

Postseismic deformation has been studied using a variety of modelling techniques, from simple layered half-space (also known as "flat-Earth") models to models that consider Earth's sphericity and three-dimensional material properties. For studying the far-field effects of earthquakes consideration of sphericity is required (Pollitz, 1992). Pollitz (1997) developed a software (VISCO1D, freely available from the USGS at: https://www.usgs.gov/software/visco1d, which contains a link to download the software) to calculate postseismic deformation on a spherical layered Earth incorporating an Earth model that varies in the radial direction only. It uses viscoelastic normal mode theory and calculates deformation from spherical harmonic expansion of global modes of relaxation. Deformation can be calculated both with and without the effect of gravity, that is, the restoring forces within the Earth allowing it to regain gravitational equilibrium. The effect of including gravity is that deformation ceases once the Earth has adjusted to the change in stress, whereas without gravity, deformation continues. This model has been employed for a wide range of earthquake studies, such as constraining Earth properties and rheological behaviour in response to the magnitude 7.9 2002 Denali earthquake in Alaska (Pollitz, 2005), computing postseismic gravity change following the magnitude 9.1 2011 Tohoko-Oki earthquake gravity change (Han et al., 2014), and modelling postseismic deformation of Antarctica (King and Santamaría-Gómez, 2016). Furthermore, VISCO1D has been used to benchmark other codes of postseismic deformation calculation (Wang et al., 2006). Whilst VISCO1D is a powerful tool, it is limited to a one-dimensional Earth model which may not be appropriate for some studies where lateral variations in Earth structure may be required to fully explain geodetic observations (King and Santamaría-Gómez, 2016).

Several finite-element models of postseismic deformation have also been developed (Freed et al., 2006; Masterlark et al., 2001; Takeuchi and Fialko, 2013), although the majority have been restricted to a ~~flat-Earth~~half-space geometry. Hu and Wang (2012) updated their ~~flat-Earth~~ finite-element model (Hu et al., 2004) to include spherical geometry and used it to study the 2004 magnitude 9.2 Sumatra earthquake, where a spherical geometry allowed for more realistic slab and fault geometry to be included, however they limited the spatial extent of the model to the case study region. Agata et al. (2019) modelled postseismic deformation following the 2011 magnitude 9.0 Tohoku-Oki earthquake with a finite-element model incorporating spherical geometry, restricting the model domain to 2500 km by 2500 km to allow for a high-resolution mesh. Whilst limiting the spatial extent is computationally efficient and does not cause a problem for the estimation of postseismic deformation, to compute a fully self-gravitational solution using spherical harmonics a full global model is required. Self-gravitation takes account of the change in gravity field caused by deformation and the redistribution of mass within the Earth. The effect of self-gravitation due to earthquake-related deformation is likely to be small for the majority of earthquakes, and not on the same scale as that caused by glacial isostatic adjustment since the magnitude of deformation is much smaller, but including it allows consistent modelling of deformation due to multiple sources (e.g. glacial cycles). Furthermore, for large earthquakes, the change in gravity field resulting from deformation and redistribution of mass within the Earth could be significant, and, if the earthquake occurs

under the ocean, redistribution of water also contributes to the change in gravity and hence affects sea levels (Broerse et al., 2011).

The purpose of the model presented in this paper is to estimate far-field postseismic deformation primarily from large earthquakes. The model is a global, spherical finite-element model constructed with the commercial software ABAQUS (https://www.3ds.com/products-services/simulia/products/abaqus/; Hibbitt et al., 2016). It is an improvement on existing models since it includes both global spherical geometry and the capability to use 3D variations in Earth properties which can significantly affect viscoelastic deformation (e.g. Latychev et al., 2005; Zhong et al., 2003) ~~and different rheological models~~. Furthermore, the model has the potential to simultaneously include different sources of Earth deformation, for example postseismic deformation in a region undergoing, or which has previously undergone, surface-mass change (e.g., ice-mass change). This is needed, for instance, to separate present-day surface deformation signals observed by GPS.

This paper describes the model setup and the methods implemented to estimate coseismic and postseismic deformation (Sects. 2 and 3). Since afterslip and poroelastic relaxation are considered only to affect deformation in the near-field of the fault for all but the largest earthquakes (Peña et al., 2019) they are not included in our model. We benchmark model results for several simple scenarios against existing codes (Sect. 4) and discuss the advantages and limitations of the model (Sect. 5). The input files are available to allow other users to replicate results and use the methods to set up their own postseismic deformation models.

2 Model Setup

2.1 Model Geometry and Mesh

The model is a global, spherical representation of the Earth, developed in ABAQUS version 2018, but is also compatible with older versions of the software as well. It is based on the finite-element model for computing glacial isostatic adjustment following the methods described by Wu (2004), whereby we use the same set up of a viscoelastic Earth relaxing in response to a stress change, but instead of applying a changing ice-surface load we implement a fault and associated slip. We model a spherical Earth rather than taking a ~~flat-Earth~~layered half-space approach so more realistic geometry can be included and gravity perturbations due to deformation can be accounted for by means of a spherical harmonic expansion. The model has layers from the surface to the core-mantle boundary with computational feasibility being the only limit on the number of layers. Each layer is assigned material properties according to user requirements and would typically consist of an elastic outer layer representing the uppermost lithosphere, with viscoelastic lower lithosphere and mantle layers below.

An earthquake is simulated in the model by movement on a fault plane within the mesh (see Sect. 3 for details) and in order to compute deformation to a sufficient accuracy a high-resolution mesh is required in the vicinity of the fault. To balance the need for a high-resolution mesh against a model with a computationally feasible number of elements, we take the approach of constructing two separate parts (ABAQUS keyword *PART): one for the high-resolution fault region and one for the lower resolution surrounding earth (Fig. 1). The two parts are then tied together (ABAQUS keyword *Tie) using surface-to-surface tie constraints. This means that although the two separate meshes have non-conforming elements relative to each other, the tie constraints ensure there is no relative movement between the surfaces and that displacement and stress are continuous through the boundaries. Tie coefficients are generated and used to interpolate quantities from nodes on one side of the mesh to nodes on the other side of the mesh. ~~which ensures that stress is transferred between the two meshes but that the two surfaces cannot penetrate each other.~~ The size of the part containing the fault and high resolution mesh can be changed according to the requirements of the individual case study, and in the simulations presented in this study, is ~~but should be~~ large enough to contain the far-field area of interest~~, for example where geodetic observations may be located~~. The high-resolution mesh block extends to 670 km depth (i.e. the base of the upper mantle) so that any deformation that may be caused by the fault movement is within the block and hence there is minimal stress to transfer across the tied surfaces. The element type used is an 8-node linear brick element (C3D8 in ABAQUS).

2.2 Rheology and Earth Parameters

All layers within the model are assigned a density (ρ), Poisson's ratio (ν) and Young's Modulus (E) (ABAQUS key words *Density *Elastic). For viscoelastic layers below the purely elastic outer shell, a relaxation time is specified which is based on a Prony time series (ABAQUS key words *Viscoelastic). In this study we limit our benchmarking examples to a 1D linear viscoelastic rheology with one (Maxwell) or two (Burgers) relaxation times, however ABAQUS has the capability of ~~using~~ implementing a variety of rheological models, including user-specified constitutive equations. For example, Freed et al. (2012) combined power-law rheology with a transient phase to model postseismic deformation following the 1999 magnitude 7.1 Hector Mine earthquake, and van der Wal et al. (2010) used a composite rheology based on laboratory-derived flow laws for diffusion and dislocation creep (Hirth and Kohlstedt, 2003; Karato and Wu, 1993) to model global glacial isostatic adjustment. Furthermore, ~~and~~ variations of our model could be constructed using a 3D Earth structure (e.g. van der Wal et al., 2015).

2.3 Boundary Conditions

We follow the approach described in Section 4.1 of Wu (2004) and apply elastic foundations (ABAQUS keyword *Foundation) to each layer boundary with a material density contrast occurring across it (including the surface and core-mantle-boundary). This means that advection of pre-stress is included and takes care of the restoring forces of buoyancy neglected in a conventional finite-element model (Wu, 2004, equation 3). The elastic foundations have a stiffness equal to the difference in density multiplied by gravitational acceleration (see Wu (2004) equations 12a,b,c). Schmidt et al. (2012) show that the use of

foundations at surfaces not perpendicular to the direction of gravity produces errors in results, but we ensure that density contrasts occur only at spherical layer boundaries in our model which satisfies this requirement. The foundations could be also replaced by spring elements when an inclined density contrast is used (Schmidt et al., 2012).

2.4 Time Steps

Once the model has been set up with the geometry, rheology, Earth parameters, boundary conditions, and fault slip (see Sect. 3); time steps are created to run the model. The first step of the run is a static step to allow the fault to slip. In this step all material properties are treated as elastic and the fault displaces immediately, hence no actual time needs to be assigned. All subsequent steps are for the simulation of postseismic relaxation and consequently must have a time assigned to them. One full run of all the time steps is one iteration.

2.5 Self-Gravitation

Movement of mass due to deformation of the Earth perturbs the gravity field which in turn affects the Earth's deformation. The effect of changes in the gravity field needs to be taken into account to make the model self-gravitating. This is done iteratively as described in Section 4.3 of Wu (2004), first using a non-self-gravitating model and computing the resulting gravitational potential from the radial displacement using the equations presented in Section 4 of~~by~~ Wu (2004). Applying this as a new load at the interfaces of the model where a density contrast occurs across them, the displacement is recalculated (i.e. another iteration is run). Wu (2004, Section 4.3) suggests running the model for 4-5 iterations to achieve convergence of the solution.

2.6 Outputs

ABAQUS can compute many different output variables depending on the model setup. For our model the main output of interest is a global grid of deformation in the east, north and radial directions. It is also possible to output stress, strain, and perturbation to the geoid which could be used to correct satellite gravimetry data for the gravity change associated with very large earthquakes (e.g. Han et al. 2014).

3 Implementation of an Earthquake

3.1 Fault Geometry and Slip

In our model an earthquake is simulated by prescribing slip on a fault plane. In order to implement this in a finite-element mesh we require two separate surfaces that can move relative to each other. We take the approach of Steffen et al. (2014), whose model simulates fault slip due to changes in stress during glacial cycles, whereby the fault plane geometry is created prior to meshing and then once generated, the mesh is subsequently altered to produce two surfaces. This is accomplished by

duplicating the nodes that lie on the fault surface and then reassigning the duplicated nodes to the elements on one side of the fault plane, thereby creating a "cut" in the mesh. Although the elements on each side of the fault are defined by different nodes, the node pairs initially have the same coordinates (Fig. 2).

The model of Steffen et al. (2014) incorporates a complex stress history comprising tectonic stresses and stresses relating to glacial cycles allowing faults to slip in response to the changing conditions. Our model differs from this approach because the amount of slip that occurs on the fault plane is prescribed. This negates the need to specify any fault surface parameters such as coefficient of friction or cohesion but does require detailed knowledge of the earthquake event. Prescribing an amount of slip on the fault plane is a reasonable approach as fault properties, such as length, width, strike, dip, rake, and slip are often solved through independent means such as fault inversion studies (Hayes, 2017) and detailed fault slip information is not required when studying far-field deformation. Furthermore, we do not include any pre-stress in the model, that is, there is no tectonic or background stress applied before the fault slips. This has no effect for models that use Maxwell or Burgers rheology as they are independent of stress.

3.2 Coseismic Slip

Once the finite-element mesh has been adjusted to accommodate the fault plane, coseismic displacement is prescribed following the approach of Masterlark (2003). For every node pair on the fault plane (i.e. nodes on either side of the fault that have the same coordinates), a third "dummy" node is created at the same location but not connected to any element in the mesh (Fig. 2). Dummy nodes are assigned a displacement boundary condition (ABAQUS keyword *Boundary) in the x and y directions of a local coordinate system aligned with the fault plane (see Fig. 2) with the amount of displacement in each direction depending on the slip and rake. For example, using basic trigonometry, a slip of 5m at a rake of -60° would equate to slip of 2.5m in the X direction and 4.3m in the Y direction. Kinematic constraint equations (ABAQUS keyword *Equation) are then constructed for each node pair and its corresponding dummy node which specifies the relative displacement between the node pair in the X and Y direction. There is no relative displacement in the Z direction of the local coordinate system (i.e. normal to the fault plane), as the fault is not allowed to open. Because the constraint equations are specified separately for each node, the fault plane can accommodate a spatially variable slip distribution. The first step of the model run is a static step (ABAQUS keyword *Static) in which the nodes (and hence the fault plane) displace according to the kinematic constraint equations. During the static step, all materials are treated as elastic.

3.3 Postseismic Deformation

Following the first step of the model run (i.e. the earthquake), the subsequent time steps simulate postseismic deformation (ABAQUS keyword *Visco) by allowing the mesh to deform under the stresses caused by the displacement on the fault plane. The kinematic constraint equations remain in place throughout the model run which means that there is no further relative displacement between the node pairs.

4 Benchmarking

In order to verify the model we benchmark the results against those produced with the Okada analytical solution for coseismic displacement (Okada, 1985) and the VISCO1D code (Version 3) for gravitational postseismic relaxation (Pollitz, 1997).

4.1 Test Setup

We perform three benchmarking tests: a strike-slip fault, a 30° dipping reverse fault, and a 45° dipping fault with rake of -60°, as summarised in Table 1. All faults outcrop at the surface of the model. The resolution of the mesh on the fault plane is 10 × 5 km. In plan view, the ABAQUS mesh has 10 km elements in the vicinity of the fault, increasing to 50 km at the edge of the fault region, with elements in the surrounding low-resolution part, starting 1000 km away from the fault, being up to 500 km (Fig. 1). The element size increases with depth as shown in Table 2. For the 30° dipping reverse fault we tested a coarser and a finer mesh and found that our chosen mesh resolution provided a satisfactory trade-off between computation time and accuracy, with the finer mesh giving only small differences in near- and far-field displacement compared to our chosen mesh, for a 10-fold increase in computation time. The results of this sensitivity test are discussed in more detail in Appendix A.

The model is run for 500 years ~~in order to~~to verify both the short and long term postseismic deformation, and for 4 iterations to ensure convergence of the self-gravitational solution. The ABAQUS input files for the benchmarking tests are included in the supplementary material (Nield, 2020). VISCO1D is run for the same time period and with maximum spherical harmonic degree of 2000, equivalent to ~10 km resolution.

In all tests the same simple Earth structure is used (details for the ABAQUS model are in Table 2), which is based on the Earth structure used by Pollitz (1997) for the upper most 670 km, and we include a uniform lower mantle layer below. We found that the vertical deformation results for VISCO1D were sensitive to the number of layers in the input Earth structure and the presence of a lower mantle, so whilst the material properties are the same for both models, the VISCO1D Earth model contains more layers. We use a simple Earth structure rather than the Preliminary Reference Earth Structure (PREM, Dziewonski & Anderson, 1981) to ensure our results are consistent with Pollitz (1997). We use a linear Maxwell rheology for all three benchmarking tests. We additionally verify the implementation of Burgers rheology against VISCO1D for the third test, with the transient viscosity (η) given in Table 2. The input files for each test case and the Earth models used in the VISCO1D modelling for both Maxwell and Burgers rheology are given in the supplementary material (Nield, 2020). All output displacement is shown normalised to the fault slip, in other words as a percentage of fault slip. This is consistent with the presentation of results by Pollitz (1997) and provides a useful metric for comparison of results. Differences between the model results are given as the difference between the percentages of fault slip.

4.2 Coseismic Results

The results of the benchmarking exercises are shown in Figs. 3-5. We show coseismic displacement in the east, north and vertical directions for a profile perpendicular to the fault strike for each of the benchmarking tests. Surface displacement is shown in Appendix B, Figs. B1-B3. The Okada analytical solution is shown by the dark green line with the equivalent ABAQUS coseismic output shown by the light green dots. The difference between the models is shown in panel b) of Figs. 3-5. Overall, there is an excellent agreement between the ABAQUS model and the Okada analytical solution. Of the three cases, the strike-slip fault agrees most closely (Fig. 3), with differences peaking at 1% of the fault slip in the north direction (Fig. 3b). There are larger differences visible for the dipping fault cases (Figs. 4-5). Some of the near-field finer details of displacement in the east and vertical directions for the dipping faults (i.e. the directions with most displacement) are not perfectly captured by ABAQUS, for example at 50 km from the fault (see Fig. 4a, vertical direction), and we attribute this ~~most likely due~~ to the mesh resolution and the distorted element shape that is required to mesh around a dipping fault. However, these differences are a maximum of 6% (Fig. 4b) and at distances greater than 300 km from the fault this decreases to less than 0.5%. Since the aim of our model is to predict far-field deformation these differences are acceptable.

4.3 Postseismic Results

Figs. 3-5 also show profiles of the postseismic displacement in the east, north and vertical directions for VISCO1D (light blue line) and the ABAQUS model (dark blue dashed line). We show displacement as a percentage of fault slip at three times: 10, 50 and 100 years after the earthquake with corresponding differences between the models shown in panel b) of each figure. Surface postseismic displacement at each of these times is shown in Appendix B, Figs. B1-B3. The ABAQUS predictions closely agree with VISCO1D for the strike-slip fault case (Fig. 3). Small differences can be observed for the dipping faults particularly in the vertical direction (Figs. 4b and 5b). ~~It is likely that t~~The mismatch in the coseismic displacement due to limitations in mesh resolution is the cause of mismatch for the postseismic displacement, ~~i.e.~~i.e., less coseismic displacement from the ABAQUS model would result in less stress and therefore less relaxation. Slight improvements in the near-field displacement could be made by increasing the mesh resolution in the vicinity of the fault but would come at a computational cost (see Appendix A). However, the differences remain small and are concentrated within 100 km of the fault with a maximum difference of 5% of the fault slip after 100 years of relaxation (Fig. 4b) and less than 0.5% at distances greater than 300 km from the fault. Therefore, we conclude that the model results are reliable for far-field postseismic deformation.

Figs. 6-7 shows displacement through time for the fault geometry in test 3 for two points at 100 km (Fig. 6) and 300 km (Fig. 7) from the fault using both a Maxwell and Burgers rheology. There is clear consistency in the evolution of postseismic relaxation between our model and VISCO1D, for both rheologies (compare solid with dashed lines on Figs. 6a and 7a). The insets in Figs. 6-7 show the results for the initial 30 years of the model run where a rapid displacement can be observed from the transient viscosity of the Burgers rheology (orange/red lines) before converging with the results from the Maxwell model

(blue lines) after approximately 30 years. Over the 500-year period, differences between our ABAQUS model and VISCO1D for the Burgers rheology are less than 0.6% of the fault slip within 100 km of the fault (Fig. 6b), or less than 0.1% at distances of 300 km or more (Fig. 7b). For the Maxwell rheology, differences peak at 0.5% of the fault slip within 100 km, reducing to 0.2% at 300 km.

5 Discussion and Conclusions

We have presented a finite-element model constructed in ABAQUS for the purposes of modelling far-field coseismic and postseismic deformation. The model is global, spherical and self-gravitating, and allows for simple modification to include three-dimensional Earth structure, non-linear rheologies and alternative or multiple sources of stress change.

The model performs well when compared with the Okada coseismic analytical solution and predictions from the postseismic VISCO1D program for all three fault scenarios we have tested. For the coseismic displacement, differences are less than 6% of the fault slip, with the largest differences in the vertical direction and near to the fault; in the fault far-field the differences are negligible. For the postseismic displacement, differences are less than 5% of the fault slip and at distances of 300 km from the fault, i.e. the far-field which is the focus of our model, this reduces to differences of 0.5%. Furthermore, we have verified that the evolution through time is an excellent match with VISCO1D for both Maxwell and Burgers rheologies.

Inclusion of self-gravitation makes only a small difference to the displacement, peaking at 0.2 mm (less than 0.1% of the fault slip) for the reverse fault (test 2) in the vertical displacement and is negligible in the horizontal directions. This demonstrates that it is not necessary to include self-gravitation when modelling postseismic deformation in isolation, but it could become important when modelling postseismic deformation alongside other larger sources of deformation such as changes in ice loading.

The main limitation of the model is that the geometry is restricted to a single fault plane within the mesh and it cannot have multiple segments of a fault plane with different strike or dip. This is due to the difficulties of constructing a valid mesh in ABAQUS with brick elements that conform to verification checks. For the same reason, including more than one earthquake in the same model would be problematic. In the case of a fault inversion that suggests multiple fault segments (e.g. Ye et al., 2014), an approximation of all the fault planes into a single geometry could still provide a realistic far-field estimate of postseismic deformation (e.g. Takeuchi and Fialko, 2013), particularly if the fault geometry and slip are adjusted so that model output matches observations of coseismic displacement (e.g. Sun et al., 2018). Far-field postseismic deformation is less sensitive to simplifications made to the fault geometry and slip distribution than near-field deformation (Khazaradze et al., 2002, Tregoning et al., 2013, Zhou et al. 2012). ~~would be required and, if constrained using near-field coseismic observations, could still provide a realistic far-field estimate of postseismic deformation.~~ Alternatively, each fault segment could be analysed

in a separate model and resulting deformation be combined, providing a linear rheology is used. The model can, however, account for varying slip and rake along the single fault plane by specifying individual values at each node pair. At present the fault is not permitted to open, and whilst this is a realistic scenario for a fault, it would have negligible impact on the far-field postseismic deformation.

We have demonstrated the validity of this model for far-field coseismic and postseismic deformations. It is an improvement on existing models as it includes global spherical geometry, self-gravitation, and can be adapted to include 3D Earth structure. It will prove particularly useful for investigating earthquakes in regions that may have large lateral variations in Earth properties where a 1D Earth model cannot reproduce geodetic observations. Furthermore, the capability of ABAQUS to model surface loading such as a changing ice load has already been established (e.g. van der Wal et al., 2010; Wu, 2004), and could easily be incorporated into this model.

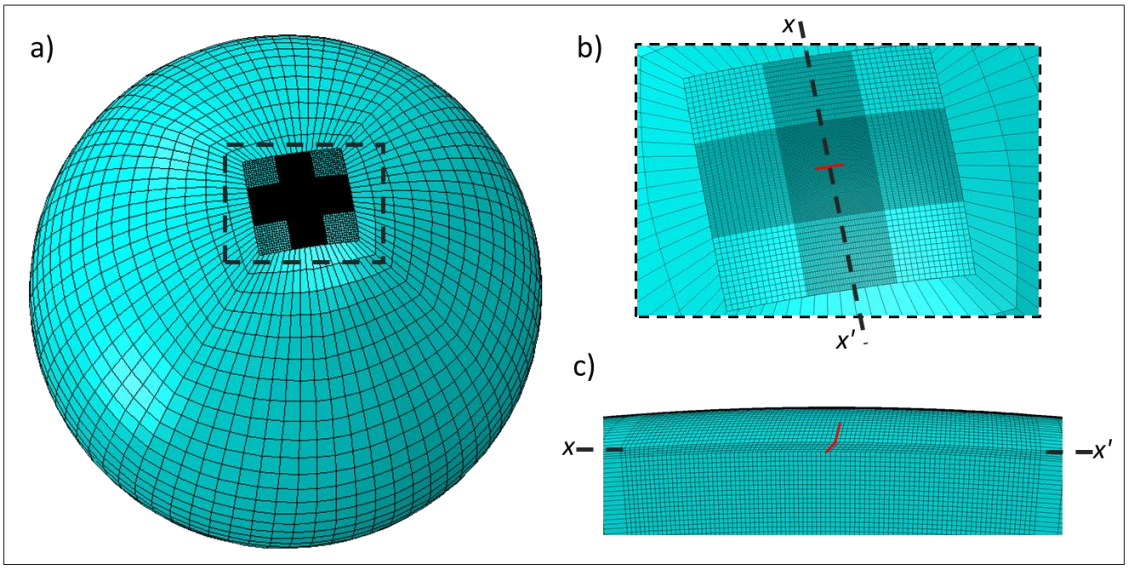

Figure 1: ABAQUS mesh; a) full global mesh with high-resolution fault region surrounded by lower resolution elements; b) close up plan view of the fault region with fault marked in red and cross-section x-x' shown in c); c) cross-section x-x' (as marked in b)) through the fault region for 45° dipping fault with fault marked in red.

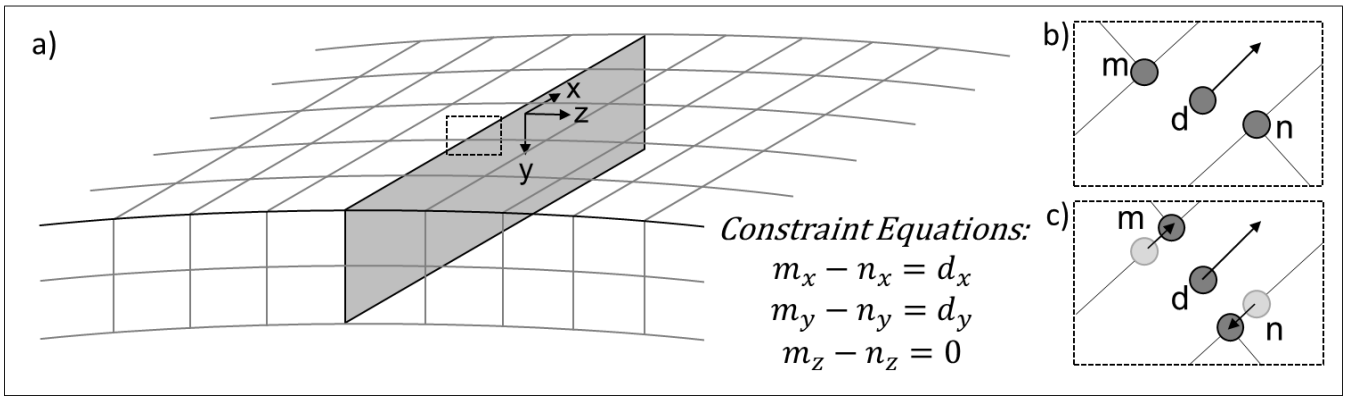

Figure 2: a) Diagram of the fault plane (shaded grey) in the ABAQUS mesh with collocated node pairs and local coordinate system aligned with the fault plane; b) close up of a node pair (m, n) and dummy node (d) with displacement boundary condition applied in the x direction of the local coordinate system (for illustrative purposes only, the fault is not allowed to open in the z direction); c) constraint equations applied to the node pair results in displacement of nodes m and n in the x direction.

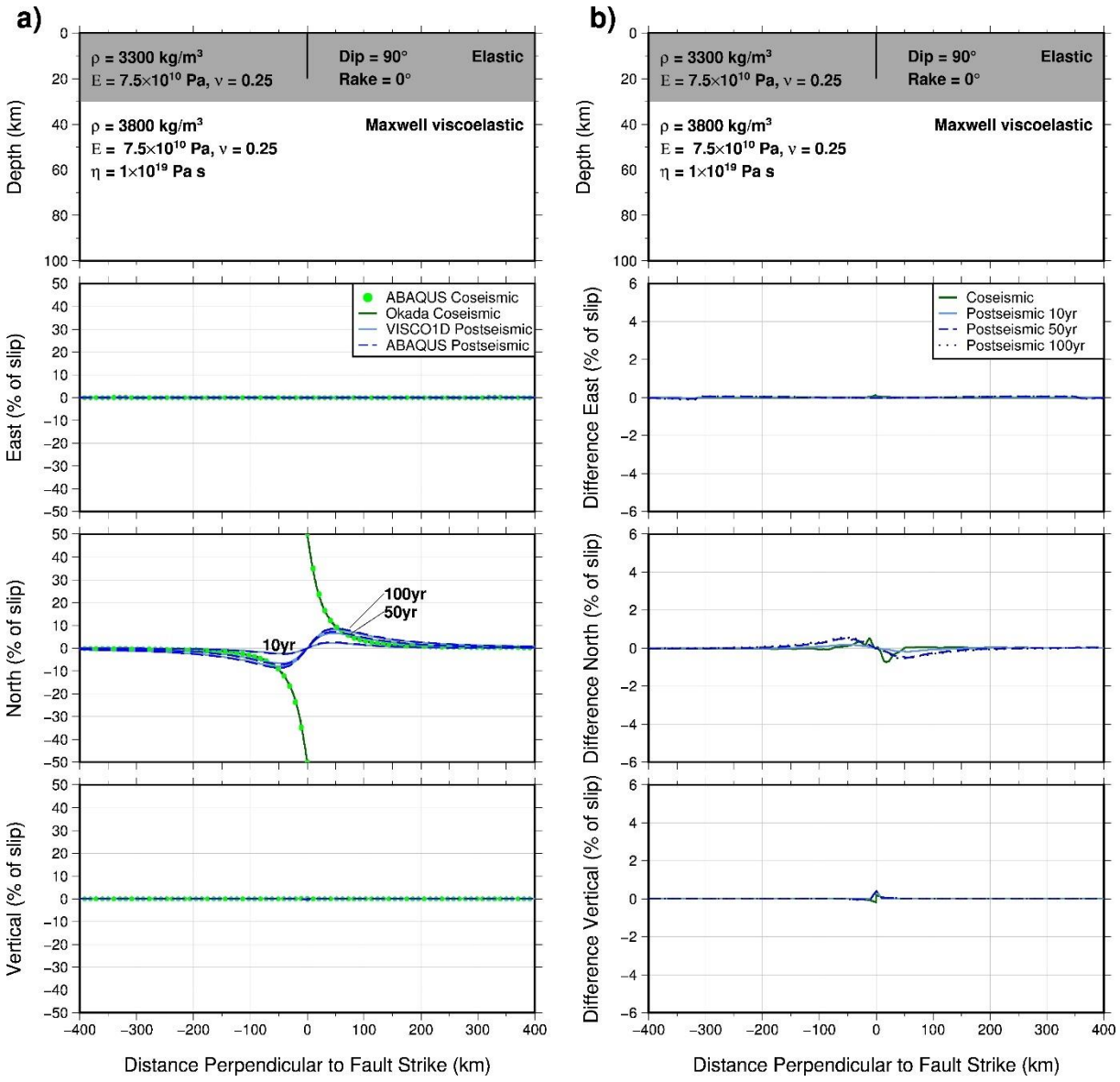

Figure 3: Top panels of a) and b) show the fault dimensions and material properties of the upper 100 km of the model. Layers and material properties below 100 km depth are given in Table 2. **a) Coseismic (green) and postseismic (blue) surface displacements in east, north and vertical directions in response to slip on a strike slip fault for a profile perpendicular to the fault strike. Results are calculated using the Okada analytical solution, VISCO1D, and ABAQUS (see legend). Postseismic displacement is shown for times 10, 50, and 100 years after fault slip. Earth properties and fault dimension are given in top panel. Displacements are given as a percentage of the fault slip. b) Differences between the ABAQUS coseismic displacement and the Okada analytical solution (green) and the ABAQUS postseismic displacement and the VISCO1D displacement (blue). Differences are in terms of percentage of the fault slip.**

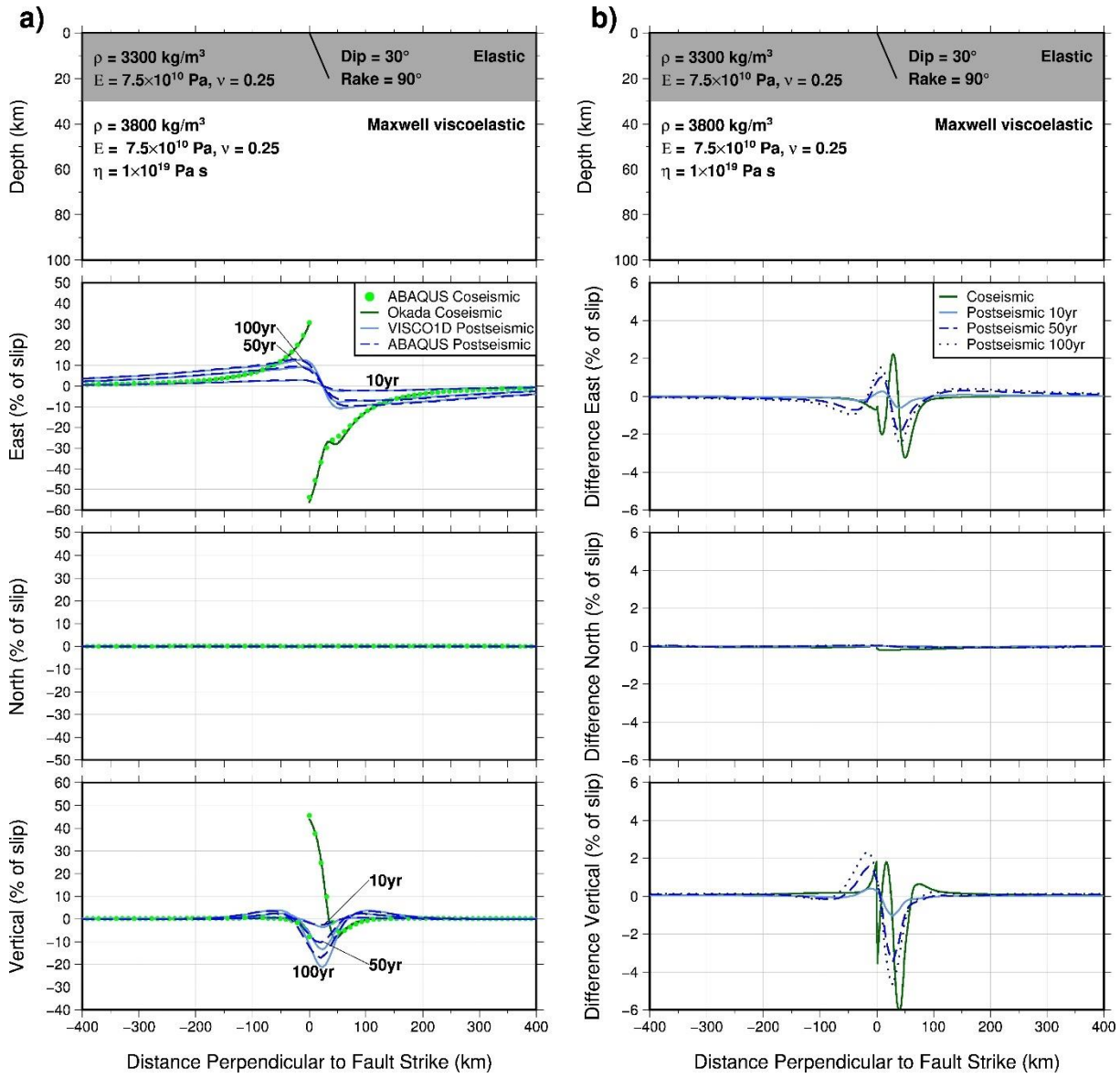

Figure 4: As for Figure 3 but for a 30° dipping reverse fault.

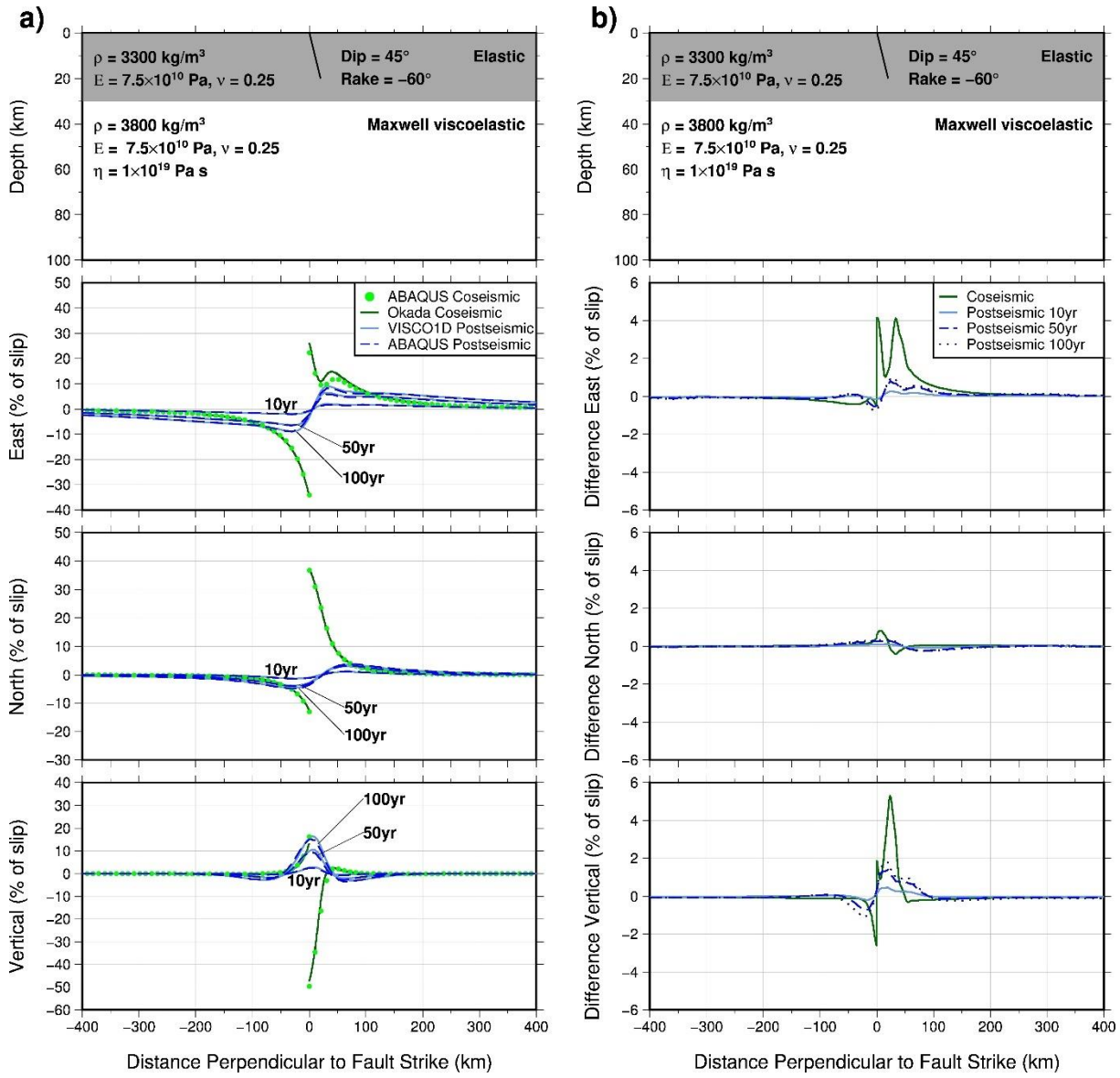

Figure 5: As for Figure 3 but for a 45° dipping fault.

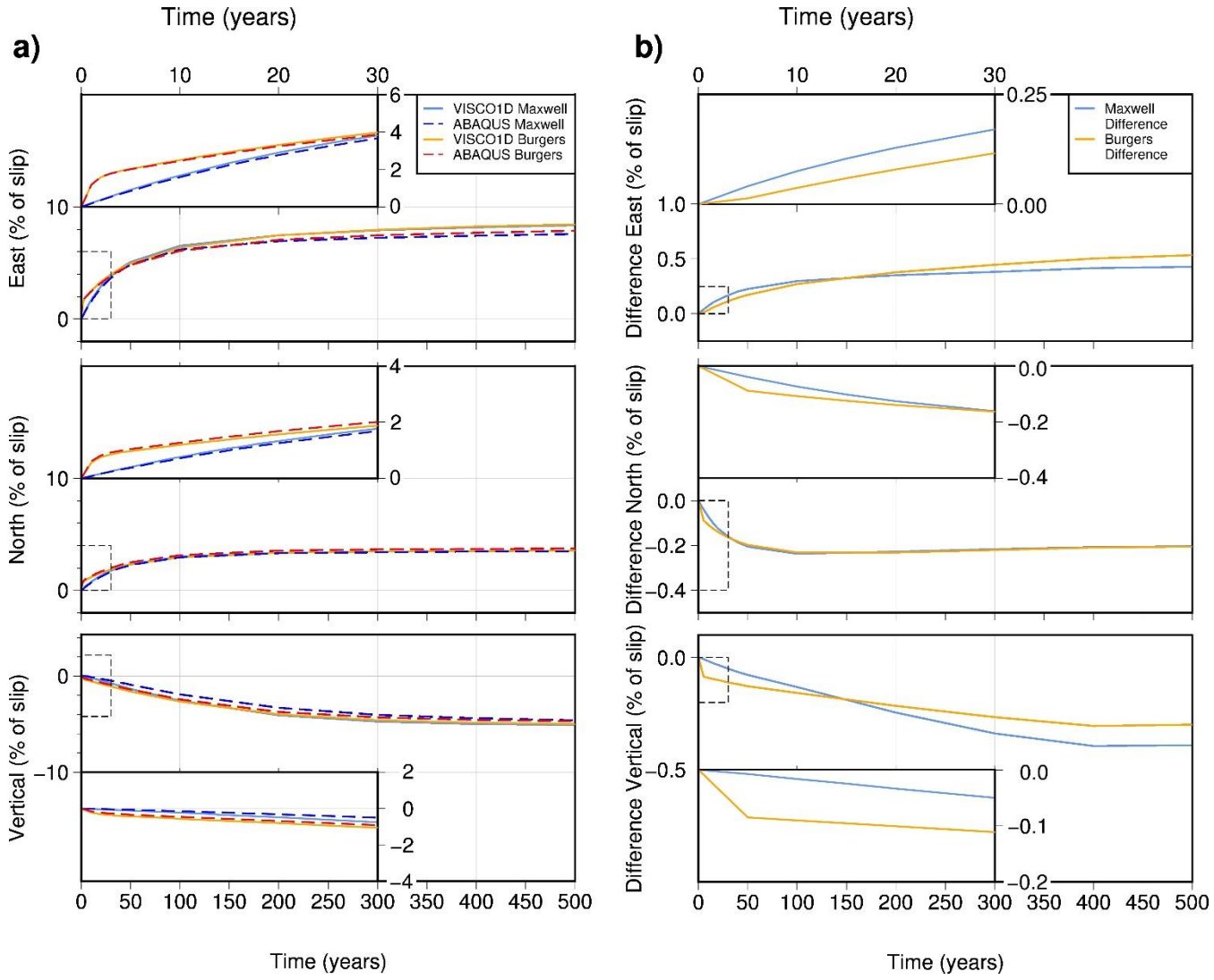

Figure 6: a) Postseismic surface displacement through time in the east, north and vertical directions at a location 100 km perpendicular to the fault in Figure 5. Predictions using two rheologies are shown: Maxwell rheology using VISCO1D and ABAQUS; and Burgers rheology using VISCO1D and ABAQUS (see legend). The main plot for each displacement direction shows 500 years of displacement with the first 30 years shown in detail in the insets. Displacements are given as a percentage of the fault slip. b) Difference between the ABAQUS postseismic displacement and the VISCO1D displacement for Maxwel rheology (light blue line) and Burgers rheology (orange line). Positive indicates ABAQUS has less displacement than VISCO1D and negative indicates ABAQUS has more displacement than VISCO1D. Differences are in terms of percentage of the fault slip. Note difference scales on the y-axis.

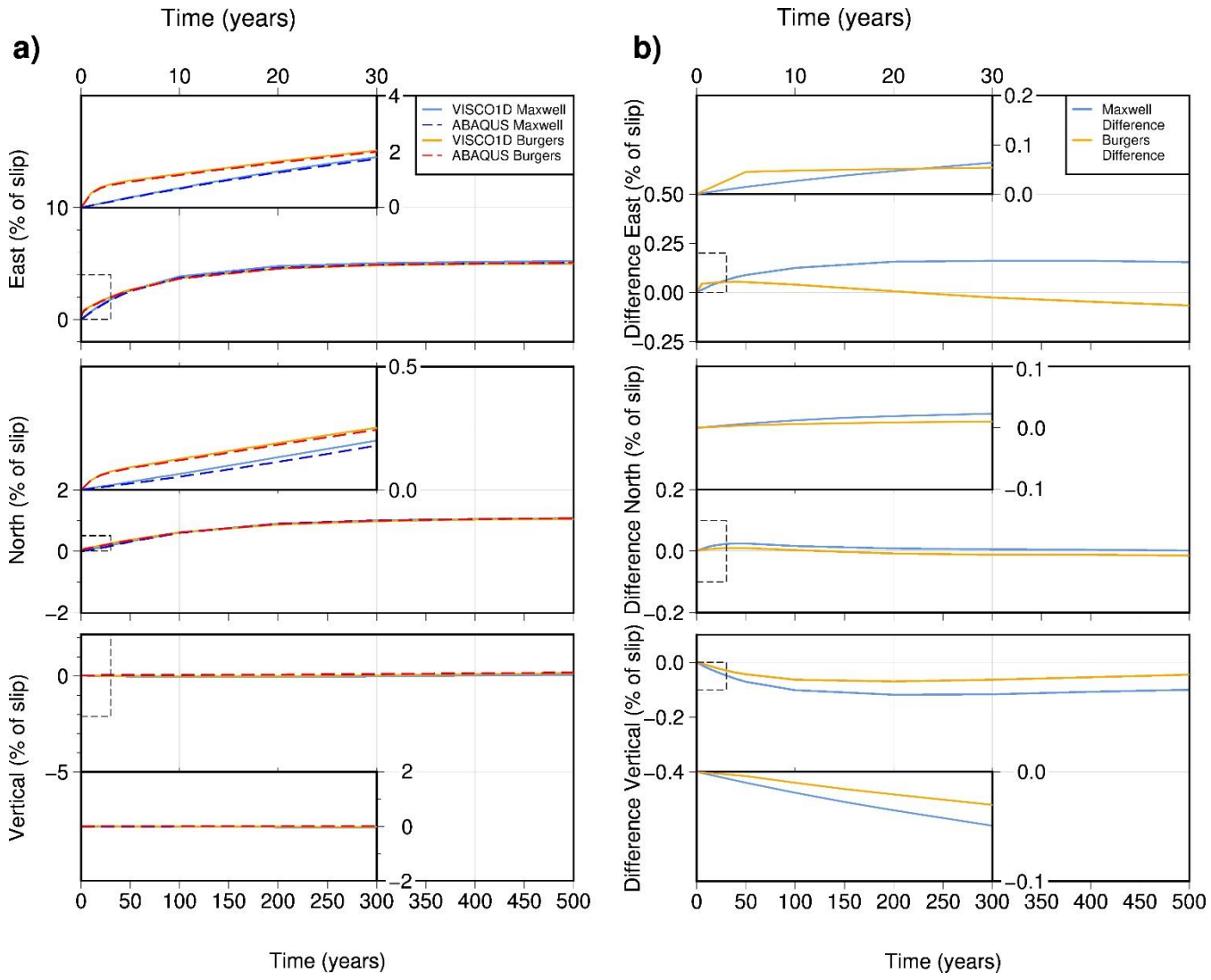

Figure 7: As for Figure 6 but for a location 300 km perpendicular to the fault in Figure 5. Note difference scales on the y-axis.

Table 1: Fault geometry used in the three benchmarking exercises.

Test	Fault length (km)	Fault width (km)	Fault vertical depth (km)	Dip (°)	Strike (°)	Rake (°)	Slip (m)
1. Strike-slip	200	20	20	90	0	0	5
2. Reverse fault	200	40	20	30	0	90	5
3. Normal oblique	200	28.28	20	45	0	-60	5

Table 2: Earth model used in the ABAQUS model for the benchmarking exercises.

Layer Description	Depth of top of layer (km)	Layer thickness (km)	Density, ρ (kg/m^3)	Young's Modulus (Pa)	Poisson's Ratio, ν	Viscosity, η (Pa s)	Vertical Element Resolution (km)
Elastic Lithosphere	0	30	3300	7.50E+10	0.25	Purely Elastic	5
Lower lithosphere/ Upper Mantle	30	6450	3800	7.50E+10	0.25	1.00E+19 (transient viscosity 1.00E+18)	10 (from 30 to 400km depth) 50 (from 400 to 670km depth)
Lower Mantle	670	2221	5000	1.10E+11	0.25	1.00E+21	500

Appendix A: Mesh Resolution Test

In general, the higher the mesh resolution the more accurate the predictions of coseismic and postseismic displacement. However, increases in the mesh resolution in the near field of the fault quickly result in a prohibitively large number of elements in the model, and it becomes computationally too expensive to run. To verify that our choice of mesh resolution is sufficient, we set up the 30° reverse fault test with a coarser and a finer mesh resolution and compared the model-predicted displacement in the near- and far-field. Since the aim of our model is to calculate far-field postseismic deformation, the convergence of displacement at distances of 300 km from the fault is what determines the choice of mesh resolution, although results are given for the near-field for interest.

Table A1 shows the resolution of each mesh along with computation time for one iteration of the model. Note, this computation time is for 8 cores on a standard Linux workstation. Due to the way ABAQUS licensing works, individual set ups may be

faster than the time quoted in Table A1 if users have access to more cores and licences. We term the mesh used in the main body of the paper the "reference mesh".

Table A1: Details of the meshes used in the sensitivity test.

	Coarse Mesh	Reference Mesh	Fine Mesh
Lateral resolution of elements on the fault plane (km)	20	10	5
Depth resolution of elements on the fault plane (km)	10	5	5
Number of elements on the fault plane	20	80	160
Number of elements in the model	161,366	417,309	1,250,590
Computation time for one iteration	45 minutes	8 hours	84 hours

We evaluate overall displacement results in terms of differences in percentage of fault slip to be consistent with Figs. 3-7. The key results are summarised in Table A2. Comparing results for the reference mesh with the coarse mesh shows that near-field coseismic differences peak at 4.5% of the fault slip and the maximum difference in the postseismic deformation after 100 years is 3.1%. When comparing the reference mesh with the fine mesh, this reduces to 1.5% for coseismic differences and 1.2% for postseismic differences.

In the far-field however, differences between the coarse mesh and reference mesh are small, peaking at 0.2% of the fault slip after 100 years of postseismic deformation. Far-field differences between the reference mesh and the fine mesh are negligible. Since the focus of our model is the far-field, these results might suggest that any of the mesh resolutions tested would be sufficient. However, in terms of absolute displacement we see an improvement from differences of 5-9 mm between the coarse mesh and the reference mesh, to 0.1-1.6 mm for differences between the reference and fine meshes. This demonstrates that results have converged at the resolution of our chosen mesh to be less than the magnitude of uncertainty associated with GPS-observed postseismic deformation (e.g., Freed et al., 2006; Wang and Fialko, 2018). We therefore conclude that the chosen mesh resolution is more than fit for purpose, with only small improvements to near-field displacement to be gained by using a finer mesh.

Table A2: Differences in displacement (expressed as percentage of fault slip) between the different meshes in Table A1. In brackets is the direction of displacement where the maximum difference is observed.

		Reference Mesh minus Coarse Mesh	Fine Mesh minus Reference Mesh
Near-field (at the fault location)	Coseismic	4.5% (vertical)	1.5% (east)
	Postseismic after 100 years	3.1% (east)	1.2% (east)
Far-field (300 km from the fault)	Coseismic	0.1% (east)	0% (east)
	Postseismic after 100 years	0.2% (east)	0.03% (east)

Appendix B

This section shows surface displacement for the ABAQUS model-predicted coseismic and postseismic displacement for each of the three benchmarking tests.

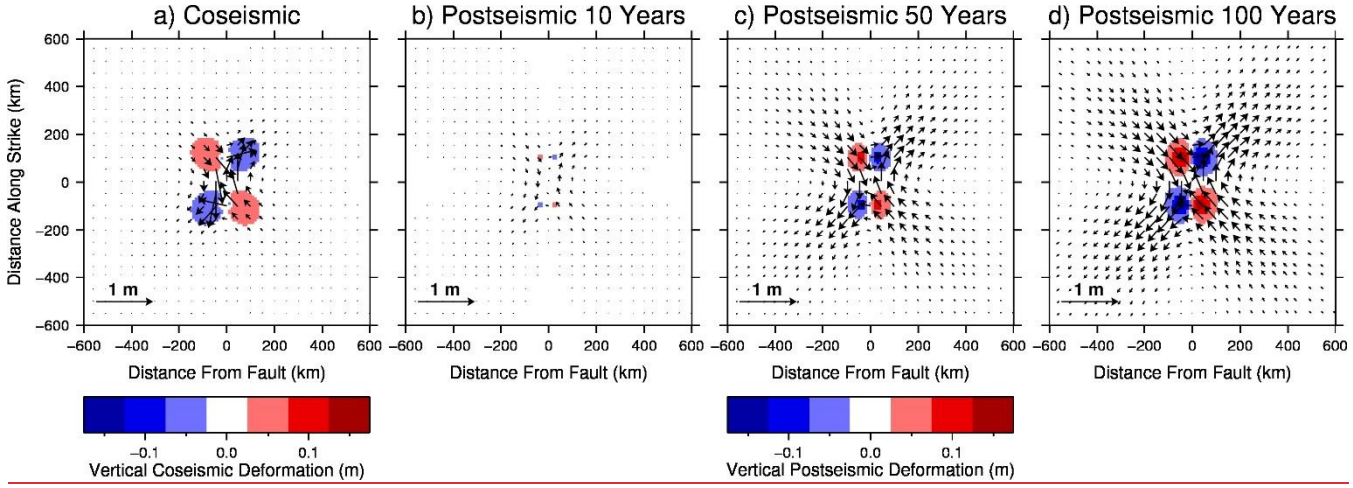

Figure B1: Model-predicted surface displacement in response to slip on a strike slip fault. Background colours show vertical displacement and arrows show horizontal displacement for: a) Coseismic displacement; b), c) and d) postseismic deformation at 10, 50, and 100 years after fault slip respectively.

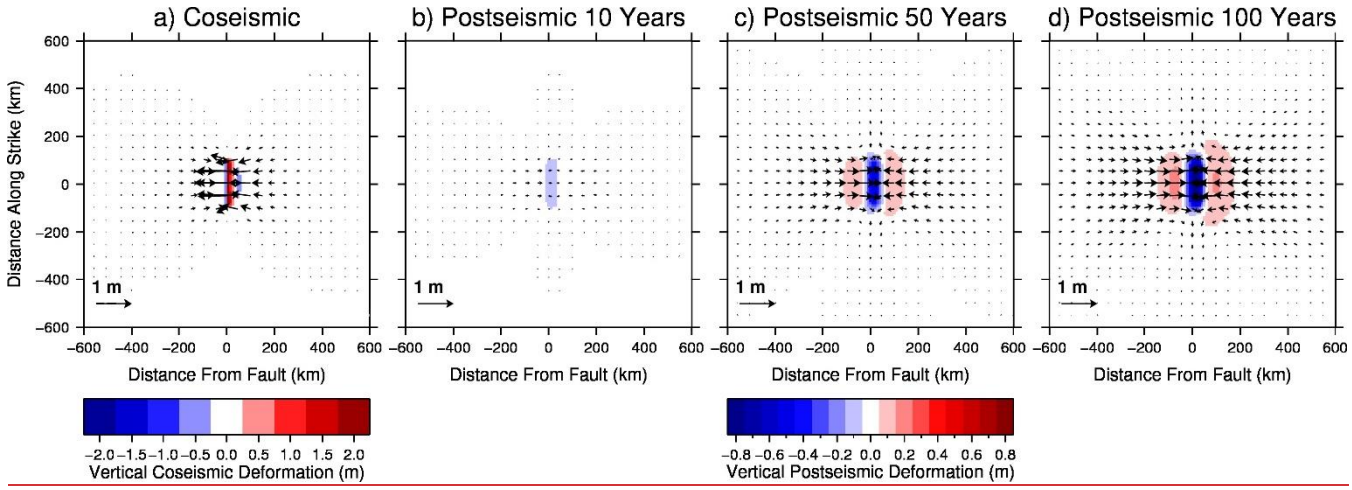

Figure B2: As for Figure B1 but for a 30° dipping reverse fault. Note the different colour scales for coseismic and postseismic displacement.

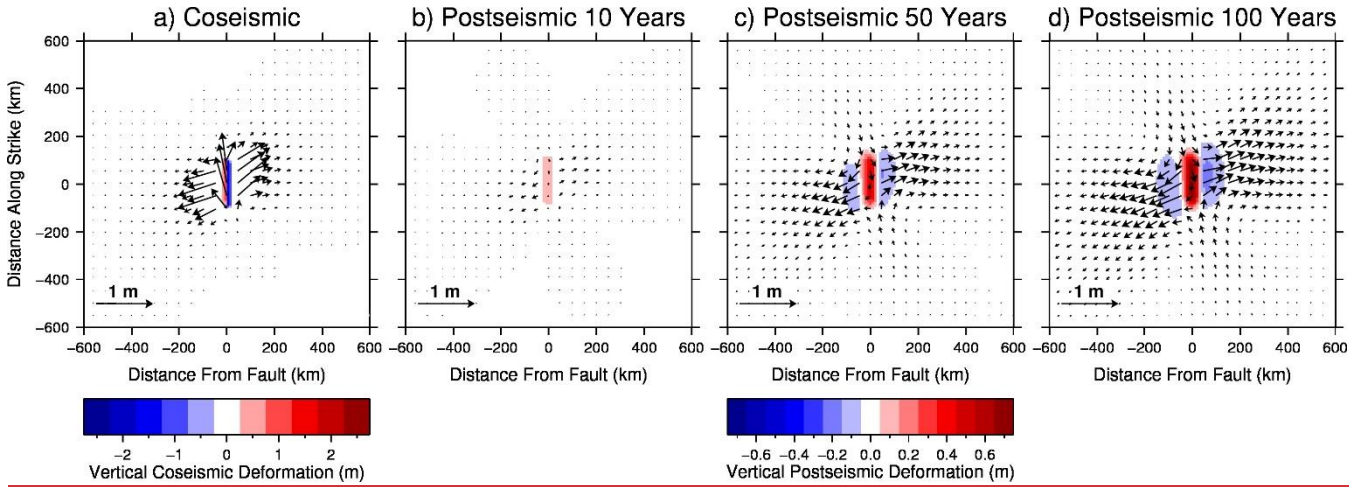

Figure B3: As for Figure B1 but for a 45° dipping fault. Note the different colour scales for coseismic and postseismic displacement.

Code Availability. ABAQUS is a commercial software and can be purchased from the developer (https://www.3ds.com/products-services/simulia/products/abaqus/), we have used version 2018 in this study, but the methods and functionality used are available in older versions of the software as well. ABAQUS input files for all four models presented in this paper are available at https://github.com/ganield/ABAQUS_Postseismic_model/releases/tag/v1.1, and archived on Zenodo: https://doi.org/10.5281/zenodo.3891444 (Nield, 2020). Instructions on how to run the files are also available at this link. VISCO1D version 3 is available for download at: https://www.usgs.gov/software/visco1d. The VISCO1D input files and

earth model files used in the experiments presented in this paper are included in the github repository, along with some instructions on how to run the code.

Author Contributions. GN developed the model. MK conceived the study and consulted in the model implementation. RS contributed meshing code for ABAQUS and consulted in the model development. BB contributed the self-gravitational part of the code. All authors contributed to the manuscript.

Competing Interests. None.

Acknowledgements. GN is supported by ARC Discovery Project DP170100224. We are grateful to Fred Pollitz for making VISCO1D freely available and for his assistance with using the software. We also thank Tim Masterlark for his advice on implementing fault slip in ABAQUS and Wouter van der Wal for guidance on constructing ABAQUS models. The handling editor Lutz Gross and two anonymous reviewers are gratefully acknowledged for their constructive comments.

References

Agata, R., Barbot, S. D., Fujita, K., Hyodo, M., Iinuma, T., Nakata, R., Ichimura, T., and Hori, T.: Rapid mantle flow with power-law creep explains deformation after the 2011 Tohoku mega-quake, Nat Commun, 10, 1385, 10.1038/s41467-019-08984-7, 2019.

Broerse, D. B. T., Vermeersen, L. L. A., Riva, R. E. M., and van der Wal, W.: Ocean contribution to co-seismic crustal deformation and geoid anomalies: Application to the 2004 December 26 Sumatra–Andaman earthquake, Earth and Planetary Science Letters, 305, 341-349, https://doi.org/10.1016/j.epsl.2011.03.011, 2011.

Dziewonski, A. M. and Anderson, D. L.: Preliminary Reference Earth Model, Phys Earth Planet In, 25, 297-356, 1981.

Freed, A. M., Burgmann, R., Calais, E., and Freymueller, J.: Stress-dependent power-law flow in the upper mantle following the 2002 Denali, Alaska, earthquake, Earth and Planetary Science Letters, 252, 481-489, 10.1016/j.epsl.2006.10.011, 2006.

Freed, A. M., Hirth, G., and Behn, M. D.: Using short-term postseismic displacements to infer the ambient deformation conditions of the upper mantle, Journal of Geophysical Research: Solid Earth, 117, 10.1029/2011jb008562, 2012.

Han, S.-C., Sauber, J., and Pollitz, F.: Broadscale postseismic gravity change following the 2011 Tohoku-Oki earthquake and implication for deformation by viscoelastic relaxation and afterslip, Geophys Res Lett, 41, 5797-5805, 10.1002/2014gl060905, 2014.

Hayes, G. P.: The finite, kinematic rupture properties of great-sized earthquakes since 1990, Earth and Planetary Science Letters, 468, 94-100, https://doi.org/10.1016/j.epsl.2017.04.003, 2017.

Hibbitt, D., Karlsson, B., and Sorenson, P.: Getting Started with ABAQUS - Version (6.14), Hibbitt, Karlsson & Sorensen, Inc. 2016.

Hirth, G. and Kohlstedt, D.: Rheology of the upper mantle and the mantle wedge: A view from the experimentalists, in: Inside the Subduction Factory, edited by: Eiler, J., Geophysical Monograph Series, AGU, 83-105, 2003.

Hu, Y. and Wang, K.: Spherical-Earth finite element model of short-term postseismic deformation following the 2004 Sumatra earthquake, Journal of Geophysical Research: Solid Earth, 117, 10.1029/2012jb009153, 2012.

Hu, Y., Wang, K., He, J., Klotz, J., and Khazaradze, G.: Three-dimensional viscoelastic finite element model for postseismic deformation of the great 1960 Chile earthquake, Journal of Geophysical Research: Solid Earth, 109, 10.1029/2004jb003163, 2004.

Huang, M.-H., Bürgmann, R., and Freed, A. M.: Probing the lithospheric rheology across the eastern margin of the Tibetan Plateau, Earth and Planetary Science Letters, 396, 88-96, https://doi.org/10.1016/j.epsl.2014.04.003, 2014.

Karato, S. and Wu, P.: Rheology of the Upper Mantle - a Synthesis, Science, 260, 771-778, 10.1126/science.260.5109.771, 1993.

Khazaradze, G., Wang, K., Klotz, J., Hu, Y., and He, J.: Prolonged post-seismic deformation of the 1960 great Chile earthquake and implications for mantle rheology, Geophys Res Lett, 29, 7-1-7-4, 10.1029/2002gl015986, 2002.

Khazaradze, G. and Klotz, J.: Short- and long-term effects of GPS measured crustal deformation rates along the south central Andes, Journal of Geophysical Research: Solid Earth, 108, 10.1029/2002jb001879, 2003.

King, M. A. and Santamaría-Gómez, A.: Ongoing deformation of Antarctica following recent Great Earthquakes, Geophys Res Lett, 43, 1918-1927, 10.1002/2016gl067773, 2016.

Latychev, K., Mitrovica, J. X., Tromp, J., Tamisiea, M. E., Komatitsch, D., and Christara, C. C.: Glacial isostatic adjustment on 3-D Earth models: a finite-volume formulation, Geophys J Int, 161, 421-444, 2005.

Masterlark, T.: Finite element model predictions of static deformation from dislocation sources in a subduction zone: Sensitivities to homogeneous, isotropic, Poisson-solid, and half-space assumptions, Journal of Geophysical Research: Solid Earth, 108, 10.1029/2002jb002296, 2003.

Masterlark, T., DeMets, C., Wang, H. F., Sánchez, O., and Stock, J.: Homogeneous vs heterogeneous subduction zone models: Coseismic and postseismic deformation, Geophys Res Lett, 28, 4047-4050, 2001.

Masterlark, T. and Wang, H. F.: Transient Stress-Coupling Between the 1992 Landers and 1999 Hector Mine, California, Earthquakes, B Seismol Soc Am, 92, 1470-1486, 2002.

Nield, G. A.: ganield/ABAQUS_Postseismic_model v1.1. Zenodo. https://doi.org/10.5281/ZENODO.3891444, 2020.

Okada, Y.: Surface deformation due to shear and tensile faults in a half-space, B Seismol Soc Am, 75, 1135-1154, 1985.

Peña, C., Heidbach, O., Moreno, M., Bedford, J., Ziegler, M., Tassara, A., and Oncken, O.: Role of Lower Crust in the Postseismic Deformation of the 2010 Maule Earthquake: Insights from a Model with Power-Law Rheology, Pure Appl Geophys, 176, 3913-3928, 10.1007/s00024-018-02090-3, 2019.

Pollitz, F. F.: Gravitational viscoelastic postseismic relaxation on a layered spherical Earth, Journal of Geophysical Research: Solid Earth, 102, 17921-17941, 10.1029/97jb01277, 1997.

Pollitz, F. F.: Postseismic relaxation theory on the spherical earth, B Seismol Soc Am, 82, 422-453, 1992.

Pollitz, F. F.: Transient rheology of the upper mantle beneath central Alaska inferred from the crustal velocity field following the 2002 Denali earthquake, Journal of Geophysical Research: Solid Earth, 110, 10.1029/2005jb003672, 2005.

Schmidt, P., Lund, B., and Hieronymus, C.: Implementation of the glacial rebound prestress advection correction in general-purpose finite element analysis software: Springs versus foundations, Comput Geosci-Uk, 40, 97-106, https://doi.org/10.1016/j.cageo.2011.07.017, 2012.

Shao, Z., Zhan, W., Zhang, L., and Xu, J.: Analysis of the Far-Field Co-seismic and Post-seismic Responses Caused by the 2011 MW 9.0 Tohoku-Oki Earthquake, Pure Appl Geophys, 173, 411-424, 10.1007/s00024-015-1131-9, 2016.

Steffen, R., Wu, P., Steffen, H., and Eaton, D. W.: On the implementation of faults in finite-element glacial isostatic adjustment models, Comput Geosci-Uk, 62, 150-159, 10.1016/j.cageo.2013.06.012, 2014.

Suito, H. and Freymueller, J. T.: A viscoelastic and afterslip postseismic deformation model for the 1964 Alaska earthquake, Journal of Geophysical Research: Solid Earth, 114, 10.1029/2008jb005954, 2009.

Sun, T., Wang, K., and He, J.: Crustal Deformation Following Great Subduction Earthquakes Controlled by Earthquake Size and Mantle Rheology, Journal of Geophysical Research: Solid Earth, 123, 5323-5345, 10.1029/2017jb015242, 2018.

Takeuchi, C. S. and Fialko, Y.: On the effects of thermally weakened ductile shear zones on postseismic deformation, Journal of Geophysical Research: Solid Earth, 118, 6295-6310, 10.1002/2013jb010215, 2013.

Tregoning, P., Burgette, R., McClusky, S. C., Lejeune, S., Watson, C. S., and McQueen, H.: A decade of horizontal deformation from great earthquakes, Journal of Geophysical Research: Solid Earth, 118, 2371-2381, https://doi.org/10.1002/jgrb.50154, 2013.

van der Wal, W., Whitehouse, P. L., and Schrama, E. J. O.: Effect of GIA models with 3D composite mantle viscosity on GRACE mass balance estimates for Antarctica, Earth and Planetary Science Letters, 414, 134-143, 2015.

van der Wal, W., Wu, P., Wang, H. S., and Sideris, M. G.: Sea levels and uplift rate from composite rheology in glacial isostatic adjustment modeling, J. Geodyn., 50, 38-48, 10.1016/j.jog.2010.01.006, 2010.

Wang, K. and Fialko, Y.: Observations and Modeling of Coseismic and Postseismic Deformation Due To the 2015 Mw 7.8 Gorkha (Nepal) Earthquake, Journal of Geophysical Research: Solid Earth, 123, 761-779, 10.1002/2017jb014620, 2018.

Wang, R., Lorenzo-Martín, F., and Roth, F.: PSGRN/PSCMP—a new code for calculating co- and post-seismic deformation, geoid and gravity changes based on the viscoelastic-gravitational dislocation theory, Comput Geosci-Uk, 32, 527-541, https://doi.org/10.1016/j.cageo.2005.08.006, 2006.

Wu, P.: Using commercial finite element packages for the study of earth deformations, sea levels and the state of stress, Geophys J Int, 158, 401-408, 10.1111/j.1365-246X.2004.02338.x, 2004.

Ye, L., Lay, T., Koper, K. D., Smalley, R., Rivera, L., Bevis, M. G., Zakrajsek, A. F., and Teferle, F. N.: Complementary slip distributions of the August 4, 2003 Mw 7.6 and November 17, 2013 Mw 7.8 South Scotia Ridge earthquakes, Earth and Planetary Science Letters, 401, 215-226, https://doi.org/10.1016/j.epsl.2014.06.007, 2014.

Zhong, S. J., Paulson, A., and Wahr, J.: Three-dimensional finite-element modelling of Earth's viscoelastic deformation: effects of lateral variations in lithospheric thickness, Geophys J Int, 155, 679-695, 10.1046/j.1365-246X.2003.02084.x, 2003.

Zhou, X., Sun, W., Zhao, B., Fu, G., Dong, J., and Nie, Z.: Geodetic observations detecting coseismic displacements and gravity changes caused by the Mw = 9.0 Tohoku-Oki earthquake, Journal of Geophysical Research: Solid Earth, 117, https://doi.org/10.1029/2011JB008849, 2012.

~~Broerse, D.B.T., Vermeersen, L.L.A., Riva, R.E.M., and van der Wal, W.: Ocean contribution to co-seismic crustal deformation and geoid anomalies: Application to the 2004 December 26 Sumatra–Andaman earthquake, Earth and Planet. Sci. Lett., 305, 341-349, 2011.~~

~~Freed, A. M., Burgmann, R., Calais, E., and Freymueller, J.: Stress-dependent power-law flow in the upper mantle following the 2002 Denali, Alaska, earthquake, Earth Planet. Sci. Lett., 252, 481-489, 2006.~~

~~Freed, A. M., Hirth, G., and Behn, M. D.: Using short-term postseismic displacements to infer the ambient deformation conditions of the upper mantle, Journal of Geophysical Research: Solid Earth, 117, 2012.~~

~~Han, S.-C., Sauber, J., and Pollitz, F.: Broadscale postseismic gravity change following the 2011 Tohoku-Oki earthquake and implication for deformation by viscoelastic relaxation and afterslip, Geophys Res Lett, 41, 5797-5805, 2014.~~

Hayes, G. P.: The finite, kinematic rupture properties of great-sized earthquakes since 1990, Earth Planet. Sci. Lett., 468, 94-100, 2017.

Hibbitt, D., Karlsson, B., and Sorenson, P.: Getting Started with ABAQUS - Version (6.14), Hibbitt, Karlsson & Sorensen, Inc. 2016.

Hu, Y. and Wang, K.: Spherical-Earth finite element model of short-term postseismic deformation following the 2004 Sumatra earthquake, Journal of Geophysical Research: Solid Earth, 117, 2012.

Hu, Y., Wang, K., He, J., Klotz, J., and Khazaradze, G.: Three-dimensional viscoelastic finite element model for postseismic deformation of the great 1960 Chile earthquake, Journal of Geophysical Research: Solid Earth, 109, 2004.

Huang, M. H., Bürgmann, R., and Freed, A. M.: Probing the lithospheric rheology across the eastern margin of the Tibetan Plateau, Earth Planet. Sci. Lett., 396, 88-96, 2014.

Khazaradze, G. and Klotz, J.: Short- and long-term effects of GPS measured crustal deformation rates along the south central Andes, Journal of Geophysical Research: Solid Earth, 108, 2003.

King, M. A. and Santamaría-Gómez, A.: Ongoing deformation of Antarctica following recent Great Earthquakes, Geophys Res Lett, 43, 1918-1927, 2016.

Masterlark, T.: Finite element model predictions of static deformation from dislocation sources in a subduction zone: Sensitivities to homogeneous, isotropic, Poisson-solid, and half-space assumptions, Journal of Geophysical Research: Solid Earth, 108, 2003.

Masterlark, T., DeMets, C., Wang, H. F., Sánchez, O., and Stock, J.: Homogeneous vs heterogeneous subduction zone models: Coseismic and postseismic deformation, Geophys Res Lett, 28, 4047-4050, 2001.

Masterlark, T. and Wang, H. F.: Transient Stress-Coupling Between the 1992 Landers and 1999 Hector Mine, California, Earthquakes, B Seismol Soc Am, 92, 1470-1486, 2002.

Nield, G. A.: ganield/ABAQUS_Postseismic_model v1.1. Zenodo. https://doi.org/10.5281/ZENODO.3891444, 2020.

Okada, Y.: Surface deformation due to shear and tensile faults in a half-space, B Seismol Soc Am, 75, 1135-1154, 1985.

Peña, C., Heidbach, O., Moreno, M., Bedford, J., Ziegler, M., Tassara, A., and Oncken, O.: Role of Lower Crust in the Postseismic Deformation of the 2010 Maule Earthquake: Insights from a Model with Power Law Rheology, Pure Appl Geophys, 176, 3913-3928, 2019.

Pollitz, F. F.: Gravitational viscoelastic postseismic relaxation on a layered spherical Earth, Journal of Geophysical Research: Solid Earth, 102, 17921-17941, 1997.

Pollitz, F. F.: Postseismic relaxation theory on the spherical earth, B Seismol Soc Am, 82, 422-453, 1992.

Pollitz, F. F.: Transient rheology of the upper mantle beneath central Alaska inferred from the crustal velocity field following the 2002 Denali earthquake, Journal of Geophysical Research: Solid Earth, 110, 2005.

Schmidt, P., Lund, B., and Hieronymus, C.: Implementation of the glacial rebound prestress advection correction in general-purpose finite-element analysis software: Springs versus foundations, Comput Geosci-Uk, 40, 97-106, 2012.

Shao, Z., Zhan, W., Zhang, L., and Xu, J.: Analysis of the Far-Field Co-seismic and Post-seismic Responses Caused by the 2011 MW 9.0 Tohoku-Oki Earthquake, Pure Appl Geophys, 173, 411-424, 2016.

Steffen, R., Wu, P., Steffen, H., and Eaton, D. W.: On the implementation of faults in finite-element glacial isostatic adjustment models, Comput Geosci-Uk, 62, 150-159, 2014.

Suito, H. and Freymueller, J. T.: A viscoelastic and afterslip postseismic deformation model for the 1964 Alaska earthquake, Journal of Geophysical Research: Solid Earth, 114, 2009.

Takeuchi, C. S. and Fialko, Y.: On the effects of thermally weakened ductile shear zones on postseismic deformation, Journal of Geophysical Research: Solid Earth, 118, 6295–6310, 2013.

van der Wal, W., Whitehouse, P. L., and Schrama, E. J. O.: Effect of GIA models with 3D composite mantle viscosity on GRACE mass balance estimates for Antarctica, Earth Planet. Sci. Lett., 414, 134–143, 2015.

van der Wal, W., Wu, P., Wang, H. S., and Sideris, M. G.: Sea levels and uplift rate from composite rheology in glacial isostatic adjustment modeling, J. Geodyn., 50, 38–48, 2010.

Wang, K. and Fialko, Y.: Observations and Modeling of Coseismic and Postseismic Deformation Due To the 2015 Mw 7.8 Gorkha (Nepal) Earthquake, Journal of Geophysical Research: Solid Earth, 123, 761–779, 2018.

Wang, R., Lorenzo-Martín, F., and Roth, F.: PSGRN/PSCMP—a new code for calculating co- and post-seismic deformation, geoid and gravity changes based on the viscoelastic-gravitational dislocation theory, Comput Geosci-Uk, 32, 527–541, 2006.

Wu, P.: Using commercial finite element packages for the study of earth deformations, sea levels and the state of stress, Geophys J Int, 158, 401–408, 2004.

Ye, L., Lay, T., Koper, K. D., Smalley, R., Rivera, L., Bevis, M. G., Zakrajsek, A. F., and Teferle, F. N.: Complementary slip distributions of the August 4, 2003 Mw 7.6 and November 17, 2013 Mw 7.8 South Scotia Ridge earthquakes, Earth Planet. Sci. Lett., 401, 215–226, 2014.